Spin models on non-Euclidean hyperlattices: Griffiths phases without extrinsic disorder

2001 J. Phys. A: Math. Gen. 34 675

(http://iopscience.iop.org/0305-4470/34/4/301)

INSTITUTE OF PHYSICS PUBLISHING JOURNAL OF PHYSICS A: MATHEMATICAL AND GENERAL

J. Phys. A: Math. Gen. **34** (2001) 675–693 www.iop.org/Journals/ja PII: S0305-4470(01)15912-3

Spin models on non-Euclidean hyperlattices: Griffiths phases without extrinsic disorder

J C Anglès d'Auriac[1], **R Mélin**[1], **P Chandra**[2] **and B Douçot**[3]

[1] CRTBT-CNRS, 38042 Grenoble Cedex, France
[2] NEC Research Institute, 4 Independence Way, Princeton, NJ 08540, USA
[3] LPTHE-CNRS UMR 7589, Universités Paris 6 et 7, 4 Place Jussieu, 75252 Paris Cedex 05, France

Received 25 July 2000, in final form 10 October 2000

Abstract

We study short-range ferromagnetic models residing on planar manifolds with global negative curvature. We show that the local metric properties of the embedding surface induce droplet formation from the boundary, resulting in the stability of a Griffiths phase at a temperature lower than that of the bulk transition. We propose that this behaviour is independent of order parameter and hyperlattice specifics, and thus is universal for such non-Euclidean spin models. Their temperature–curvature phase diagrams are characterized by two distinct bulk and boundary transitions; each has mean-field critical behaviour and a finite correlation length related to the curvature of the embedding surface. The implications for experiments on superconducting hyperlattice networks are also discussed.

PACS numbers: 7510, 0520, 0545, 0550

1. Introduction

Disordered spin systems behave in ways qualitatively distinct from their periodic counterparts [1–3]. More specifically, they display broad relaxation spectra, in clear contrast to the Debye relaxation observed for spin crystalline materials. Relaxation times depend on local conditions, and thus it is not surprising that randomly coupled spins relax on a wide distribution of timescales. There are now several anomalous magnetic materials [4–6], whose non-Debye relaxation seems to be determined by lattice topology [7] rather than by disorder. The theoretical challenge is to identify and characterize regular reductionist models that exhibit such behaviour in the absence of intrinsic randomness.

There are several analytic studies of periodic glass models [8], though their infinite-range nature makes their relevance to real materials unclear. More specifically, the absence of any length scale in these approaches implies relaxation on just a few timescales. Detailed analytic methods to treat short-range glasses, even with intrinsic disorder, remain to be found. It has been proposed that their slow dynamics result from rare, locally ordered spatial regions that are energetically probable due to random spin–spin couplings [9, 10], similar

0305-4470/01/040675+19$30.00

to the situation associated with Griffiths phases [11, 12] in diluted ferromagnets; here large fluctuating droplets lead to relaxation on long timescales. Though the application of this droplet scenario to experimental spin glasses remains controversial [13], it is an appealing starting point for geometrically induced glassiness. In quenched ferromagnets, the random initial configuration approaches equilibrium via domain wall motion [14]. This coarsening occurs more slowly when the boundaries are pinned by impurities, as is the case in the random-field Ising model [15]. Thus one can ask whether local geometry can induce such slow domain wall dynamics for a short-range ferromagnetic model. Self-similar lattices are excellent candidates, since all minority droplets will be non-compact [16]; indeed non-trivial slow relaxation has been reported in this case [17, 18]. It is therefore natural to continue this program by studying ferromagnets on lattices embedded in surfaces with constant negative curvature. Dynamics on such hyperbolic manifolds, particularly in the area of chaos [19, 20], are known to be qualitatively similar to those observed in disordered systems [21] and thus such surfaces provide promising settings for the identification of broad relaxation spectra in disorder-free models.

In this paper we show that regular ferromagnetic models on hyperlattices with open boundary conditions exhibit slow dynamics on a distribution of timescales in the absence of intrinsic randomness. Their metric structure makes it energetically probable for large domains of minority spins to nucleate at the boundaries, leading to the stability of a Griffiths phase at a temperature lower than the bulk temperature. In dilute ferromagnets with correlated disorder, the presence of such rare droplets leads to a diverging magnetic susceptibility [24], a phenomenon that we also observe for the regular hyperlattice models. We attribute this behaviour to the distinction between bulk and boundary sites, where the latter comprise a significant proportion of the total site number. Two mean-field transitions are identified, associated with the bulk and the boundary respectively, whose characters are determined by local metric properties; for example the correlation length associated with each transition is related to the curvature of the embedding surface. We conjecture that this phase behaviour is universal for *all* short-range ferromagnetic models residing on lattices embedded on hyperbolic planes, independent of details associated with the spin order parameter or lattice specifications.

The outline of this paper is as follows. In the next section (section 2) we discuss geometrical properties of lattices embedded in surfaces of negative curvature. The model and its specific heat are presented in section 3. The Bethe–Peierls transition for the central spin, that which is deepest in the hyperlattice, is derived in section 4. This analysis is generalized in section 5 to an arbitrary lattice site. Analysis of magnetization distributions is presented in section 6, with particular emphasis on the inferred slow dynamics. In section 7, we summarize our results with a conjectured phase diagram for these models in the curvature–temperature plane and discuss possible experiments on Josephson junction arrays. In order to maintain the flow of the text, we have delegated the derivation of the main analytical results to appendices.

2. Hyperlattices: regular lattices on a hyperboloid

Infinite regular lattices are characterized by two integers (p, q), where p is the number of polygon edges and q is the number of polygons around a given vertex. On an Euclidean plane (i.e. no curvature), there are three tilings corresponding to $(p-2)(q-2) = 4$: the square (4, 4), the triangular (3, 6) and the honeycomb (6, 3) lattices. On the sphere $\mathcal{S}_2$ (positive curvature) the five platonic polyhedra correspond to the condition $(p-2)(q-2) < 4$: the tetrahedron (3, 3), the cube (4, 3), the octahedron (3, 4), the dodecahedron (5, 3) and the icosahedron (3, 5). Hyperlattices, tilings of the hyperbolic plane with negative curvature, correspond to the

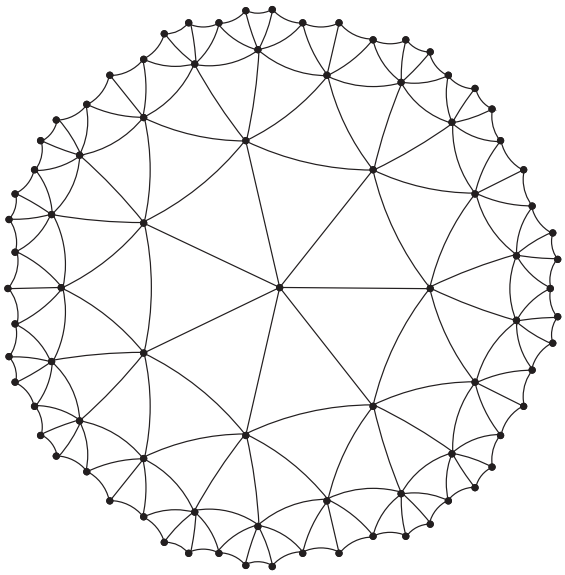

Figure 1. The site-centred (3, 7) hyperlattice with three generations.

condition $(p-2)(q-2) > 4$; clearly there exist an infinite number of possibilities. The site-centred (3, 7) hyperlattice is shown in figure 1.

Loopless trees, such as Bethe lattices, correspond to regular tilings of the hyperbolic plane labelled by the integers (∞, q) [25, 26]. Hyperlattices can be built in a shell structure, where each layer is analogous to a generation of a tree. For a hyperlattice of n shells, the number of boundary sites, δV_n, scales with the number of bulk sites, V_n; since $\delta V_n \sim V_n^{1-\frac{1}{D}}$ for a Euclidean tiling in D dimensions, the hyperlattices are considered to have $D = \infty$. However they possess intrinsic length scales determined by their radii of curvature, a feature that influences the critical behaviour of models residing on these surfaces [27].

It is useful to study the continuous-space analogue of the hyperlattice, represented as a unit disc on the Lobachevskii plane with a metric

$$g(z) = \frac{1}{(1-|z|^2)^2} \tag{1}$$

where $z = x + \mathrm{i}y$ is a point on the disc. A finite-size system is obtained by restricting z to the disc $|z| < R < 1$. The minimum-length paths, e.g. the geodesics, between two points at coordinates z_1 and z_2 are circles perpendicular to the unit circle. The distance between z_1 and z_2 is

$$d(z_1, z_2) = \tanh^{-1}\left|\frac{z_1 - z_2}{1 - z_1\bar{z}_2}\right|. \tag{2}$$

In order to illustrate the phenomenology associated with different curvatures, we determine the short-scale corrections to the perimeter of a circle, $\mathcal{L}$, of radius d for the negative and positive cases. First we consider the circle embedded on a two-dimensional sphere where its perimeter is decreased by the presence of a *positive* curvature $\mathcal{R}$:

$$\mathcal{L}_{\mathcal{S}^2} = 2\pi d - \frac{\pi}{3\mathcal{R}^2}d^3 + \cdots. \tag{3}$$

We can perform an analogous expansion for the case of the hyperbolic plane with the metric

equation (1). The set of points at a fixed distance d from a given point X (chosen on the real axis) is found to be represented by the circle $z = x_0 + R_0 \exp(\mathrm{i}\phi)$, with

$$x_0 = X\frac{1-\tanh^2 d}{1-X^2\tanh^2 d} \qquad \text{and} \qquad R_0 = (1-X^2)\frac{\tanh d}{1-X^2\tanh^2 d}. \tag{4}$$

The periphery of the circle $z = x_0 + R_0 \exp(\mathrm{i}\phi)$ is

$$\mathcal{L}_{\text{bulk}} = \int_0^{2\pi} \sqrt{g(z)}R_0\,\mathrm{d}\phi = \pi \sinh(2d) \tag{5}$$

so that a short-scale expansion to order d^3 leads to

$$\mathcal{L}_{\text{bulk}} = 2\pi d + \frac{4\pi}{3}d^3 + \cdots. \tag{6}$$

Comparing equation (6) with (3), we see that the perimeter of a circle of radius d is larger (smaller) than $2\pi d$ on a surface with a negative (positive) curvature. Identifying the corrections to $2\pi d$, we see that the curvature associated with the metric equation (1) is $\mathcal{R} = -1/2$. On large length scales, the sphere is compact; there are no more points at a distance larger than a critical value. By contrast, on the manifold with negative curvature, the number of points at a distance d from a given point increases exponentially with d above the curvature radius:

$$\mathcal{L}_{\text{bulk}} \sim \frac{\pi}{2}\exp(2d) \tag{7}$$

which is obtained from equation (5). On a Bethe lattice, the number of points at a given distance d scales as z^d, with z the branching ratio. This indicates a close link between the tree and hyperlattice structures, related to the underlying manifold with negative curvature.

3. The free energy of the hyperlattice model

Here we study the nearest-neighbour ferromagnetic Ising model (FIM) with Hamiltonian $\mathcal{H} = -\sum_{\langle i,j\rangle}\sigma_i\sigma_j$, where $\sigma = \pm 1$ and $\langle i, j\rangle$ are neighbouring sites on a hyperlattice. A characterization of a special case, the FIM on the Cayley tree, has already been reported [17,22,23]. However there exists a temperature scale, T_{g}, below which large droplets of flipped spins proliferate from the boundaries, resulting in non-Gaussian magnetization and glassy behaviour for a macroscopic number of sites. In this paper we investigate such boundary-induced Griffiths phases for spin models on more general hyperlattices.

The free energy per spin of the FIM on the Cayley tree is analytic for all temperatures; because of the absence of loops on this pseudo-lattice, it can be obtained from a high-temperature series expansion and is $f(\beta) = -2\ln[\cosh(\beta)]$. The situation could be different for a general hyperlattice due to the presence of loops. The number of independent cycles n_{c} of a graph with n_{s} sites and n_{b} of bonds is $n_{\text{c}} = n_{\text{b}} - (n_{\text{s}} - 1)$. For the (3, 7) hyperlattice, we have $n_{\text{c}}/n_{\text{s}} \sim (5-\sqrt{5})/2 \approx 1.381\,97$, which is even larger than the square lattice value $n_{\text{c}}/n_{\text{s}} = [2L^2 - (L^2-1)]/L^2 \sim 1$. Thus the free energy of the FIM on the hyperlattice could have a singularity, and its absence/presence must be checked explicitly. In order to do this, we have measured its internal energy $\langle e\rangle$ and specific heat $c_v = (\langle e^2\rangle - \langle e\rangle^2)/T^2$ using numerical simulations. We have ensured that the equilibrium distribution was properly sampled by comparing the numerical estimate of $\mathrm{d}\langle e\rangle/\mathrm{d}T$ and $(\langle e^2\rangle - \langle e\rangle^2)/T^2$ and have used both heat-bath and cluster algorithms [28], with perfect agreement. The temperature dependence of the specific heat is shown in figure 2 for an increasing number of layers $n = 8, 11, 12$. All these curves display a maximum around the same temperature, but these peaks do *not* increase with the system size (the number of sites is increased by 50 between eight and 12 layers whereas the

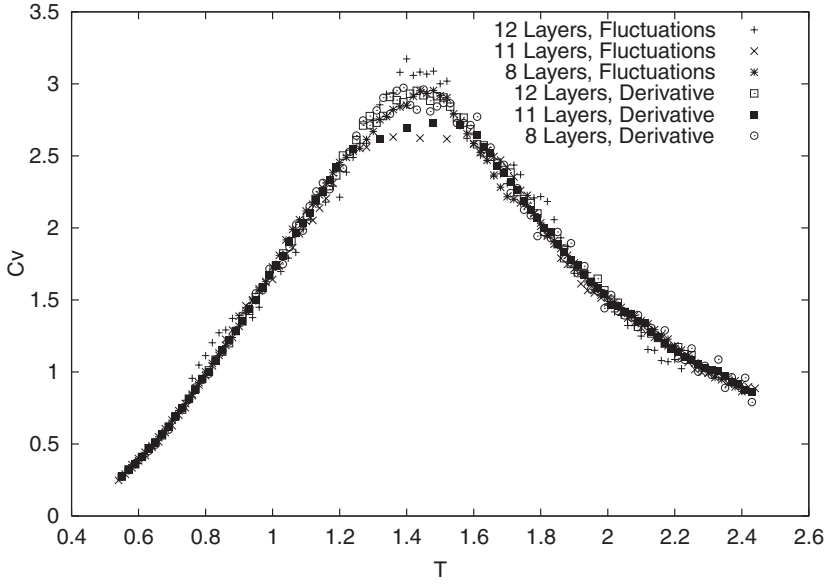

Figure 2. Specific heat for a (3, 7) hyperlattice computed from the numerical derivative of the internal energy and from the fluctuation of energy. The agreement indicates that thermal equilibrium is properly sampled. The results presented are obtained with eight, 11 and 12 layers. The number of sites is 4264 (eight generations), 76 616 (11 generations) and 200 593 (12 generations). The number of bonds is 10 150 (eight generations), 182 490 (11 generations) and 477 799 (12 generations). No sign of divergence is found when the system size is increased.

specific heat remains identical up to the statistical noise); thus we interpret this maximum as a Schottky anomaly rather as a signature of a sharp phase transition in the thermodynamic limit. The free energy of the FIM on the hyperlattice thus appears to be analytic at all temperatures, similar to the situation for the special case of the Cayley tree. We note that here we are always considering the case of open boundaries.

4. The Bethe–Peierls transition of the central spin

In order to characterize the behaviour of the FIM on a hyperlattice, we begin by considering the ordering of its central spin, that residing on the site deepest in the lattice (e.g. the site $\mathcal{T}_0$ in figure 3). As a point of reference, we review the special case of the Cayley tree where the central spin is known to undergo a mean-field Bethe–Peierls transition [29–33]. In response to an applied uniform field on the entire tree, its central spin develops the local susceptibility χ_0^{tree}

$$T\chi_0^{\text{tree}} = \sum_l \exp\left(-\frac{d_l}{\xi_{\text{T}}}\right) = \sum_{n=0}^{+\infty}(z-1)^n \exp\left(-\frac{n}{\xi_{\text{T}}}\right). \tag{8}$$

Here we use the subscript '0' in χ_0^{tree} to emphasize that we are *only* considering the behaviour of the central spin. In equation (8), d_l is the distance between the central site $\mathcal{T}_0$ and the site l; $\xi_{\text{T}} = -1/\ln(\tanh(\beta J))$ is the correlation length set by the exponential decay of the spin correlations $\langle\sigma_k\sigma_l\rangle \sim \exp(-d_{k,l}/\xi_{\text{T}})$, identical to that of the Ising chain because of the absence of loops. The central spin susceptibility χ_0^{tree} diverges if $T < T_{\text{BP}}$, with $(z-1)\tanh(\beta_{\text{BP}}J) = 1$. We emphasize that this transition results from the metric of the embedding curved space, which leads to the prefactor $(z-1)^n$ in equation (8); this is the number of sites at generation n from the

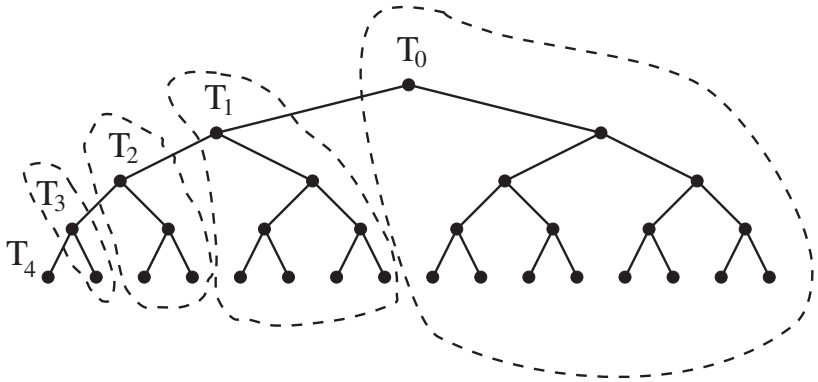

Figure 3. A tree with four generations and a forward-branching $z-1=2$. We denote by $\mathcal{T}_0 \ldots \mathcal{T}_n$ the vertices along a path from the top site to a leaf site. The sites descendent from a given vertex $\mathcal{T}_m$ are grouped together as shown on the figure to calculate the generalized Bethe–Peierls susceptibility in section 5.

central spin. Thus, thanks to this prefactor, exponentially decaying correlations are sufficient to generate mean-field ordering of the central spin. As an aside, we note that here we have only considered χ_0^{tree}, but this calculation can be generalized to characterize the full thermodynamic behaviour associated with this spin [32, 34].

For the FIM on the general hyperlattice with loops, the expression for the local susceptibility is also dominated by the long-length-scale contribution of the spin–spin correlations, leading to a diverging susceptibility with a finite correlation length [27]. Equation (8) may be adapted to evaluate the central-spin susceptibility using a continuous-space description

$$T\chi^{\text{lob}}(0) = \int_{|z|<R} g(z) \exp\left(-\frac{d(z,0)}{\xi_{\text{T}}}\right) \mathrm{d}^2 z \tag{9}$$

where $g(z)$ is the metric in equation (1), and $d(z,0)$ is the distance between the origin and the site at $z = \rho \exp(\mathrm{i}\theta)$ (see equation (2)). We have implicitly identified the distance on the graph and the 'hyperbolic' distance given by the metrics. In fact, for a given distance on the graph, there is a Gaussian distribution of hyperbolic distances, which has been studied in detail for a Cayley tree model by Comtet *et al* [21]. We claim that the physics of the FIM is not sensitive to the existing difference between the two distances. The resulting susceptibility

$$T\chi^{\text{lob}}(0) = 2\pi \int_0^R \left(\frac{1+\rho}{1-\rho}\right)^{-1/(2\xi_{\text{T}})} \frac{\rho}{(1-\rho^2)^2}\, \mathrm{d}\rho \sim \frac{1}{T - T_{\text{BP}}}$$

diverges when $\xi_{\text{T}} = 1/2$, with the mean-field exponent $\gamma = 1$. In fact, all the critical exponents of the Bethe–Peierls transition are mean field. This can be seen in the following manner: on d-dimensional Euclidean lattices, the upper critical dimension of spin models is related to the probability of intersecting random walks [35]. On hyperlattices (including the special case of trees), the return probability of a random walk is vanishingly small [36–39], indicating that FIM hyperlattice models are above their upper critical dimension, and thus mean-field transitions are expected.

5. Generalized Bethe–Peierls transitions

We would like to consider a possible Bethe–Peierls transition for an arbitrary spin of the FIM on a general hyperlattice. Again, we begin by studying the special case of loopless Cayley trees. Here we consider spin ordering on an arbitrary site $\mathcal{T}_m$ at generation $m = 0, \ldots, n$ (see figure 3). We group the sites, indicated in figure 3, to expand the susceptibility in powers of $x = \tanh(\beta J)$ (for details see appendix A) to obtain

$$T\chi_m^{\text{tree}} = \frac{1-[(z-1)x]^{n-m+1}}{1-(z-1)x} + x\frac{1-x^m}{1-x} + \frac{(z-2)x^2}{1-(z-1)x}\left[\frac{1-x^m}{1-x} - [(z-1)x]^{n-m+1}\frac{1-[(z-1)x^2]^m}{1-(z-1)x^2}\right]. \tag{10}$$

In the limit $n, m \to +\infty$ and $n - m$ constant (boundary behaviour), $\chi_m^{\text{tree}}(T)$ is smooth at the Bethe–Peierls transition temperature ($(z-1)\tanh(\beta_{\text{BP}}J) = 1$), but diverges at a lower temperature T' corresponding to $(z-1)\tanh^2(\beta' J) = 1$. As shown explicitly in appendix A, the existence of this transition results from a combination of the local metric (i.e. the number of sites a distance from the reference one) and exponential spin correlations. In the limit $n \to +\infty$ and m fixed (bulk behaviour), χ_m^{tree} in equation (10) diverges at the Bethe–Peierls temperature T_{BP} with mean-field behaviour. If $n \to +\infty$ and $m = \lambda n$, with λ kept fixed, the susceptibility in equation (10) shows a divergence at the Bethe–Peierls temperature. The temperature T' has already been found by several authors by studying the magnetic field dependence of the Potts model on the Cayley tree [40, 41]. Here, we provide another interpretation for this transition, in terms of a local Bethe–Peierls transition controlled by the metric properties at the boundary, and prove that this transition is related to a Griffiths phase.

We have therefore demonstrated the existence of two *distinct* Bethe–Peierls transitions associated with the bulk (where $n - m \to +\infty$), and the boundary, related to the different metric properties associated with these two different site species. They also affect percolation thresholds on these trees, as discussed in appendix B.

Now that we have understood the bulk and boundary transitions of the tree FIM in terms of metric properties, we continue to ask a similar question about their more general hyperlattice analogues. We stress that, on these manifolds of negative curvature, site scaling is different for reference sites in the bulk and on the boundary. As displayed in equation (7), the number of sites at a distance d from a given bulk reference one scales as $\mathcal{L}_{\text{bulk}} \sim (\pi/2)\exp(2d)$ in the continuous-space model. In appendix C we show that the analogous quantity associated with a boundary reference site scales as $\mathcal{L}_{\text{bound}} \sim \exp(d)$. This result is compatible with our numerical determination of the site scaling at a given distance, as displayed in figure 4.

The expression for the local susceptibility involves a correlation length, which is not necessarily uniform for the full lattice. We assume a uniform, isotropic correlation length as an ansatz and then deduce the existence of bulk and boundary transitions for the general hyperlattice set by $\xi_{\text{T}} = 1/2$ (see section 4) and by $\xi_{\text{T}} = 1$. The existence of two different transitions does not rely on the initial *ansatz* because the correlation length at the boundary can only be reduced compared to that of the bulk. Therefore, the initial *ansatz* of uniform correlations indicates the existence of a boundary transition at a temperature lower than the bulk transition.

We support the previous analysis, assuming a uniform spin correlation length, with numerical determinations of the spin–spin correlations. On the Cayley tree, the correlation of two spins σ and σ' at a distance d is $[\tanh(\beta d)]^d$, irrespective of the site locations of the two reference spins. By contrast, as discussed below, the situation is different for the general hyperlattice case where the correlations are reduced at the boundary. We distinguish between spin correlations in the bulk and at the boundary.

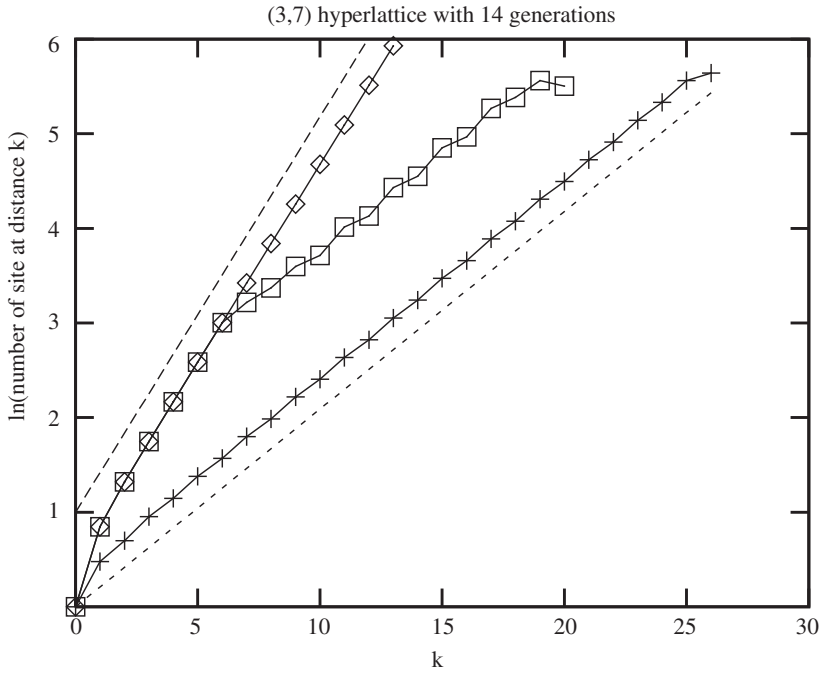

Figure 4. Logarithm of the number of sites of the (3, 7) hyperlattice with 14 generations as a function of distance k from a given site located (i) at the centre of the hyperlattice (diamonds) where the calculated exponential growth is indicated by a dashed line, (ii) on the boundary (crosses) with calculated exponential growth (short dashed line) that is the square root of the calculated bulk growth (dashed line) and (iii) on an intermediate (7) generation (boxes), where a crossover is observed between bulk and boundary behaviour with increasing distance scales.

Bulk. The symmetry group of the (3, 7) hyperlattice with a finite number of layers n is generated by one rotation of angle $2\pi/7$ around the central spin, and one inversion with respect to an axis going through the central spin. The infinite hyperlattice has a huge symmetry group: the lattice is left invariant under the aforementioned set of symmetries around *any* lattice site, a fact that is no longer true for a finite system. However the properties of the finite-size lattice reflect the huge symmetry of the infinite lattice. To be more precise, let us consider a FIM on a hyperlattice with n layers and N_k correlations $\langle\sigma_0\sigma_k\rangle$ between a given spin σ_0, and any of the N_k spins at a distance k from σ_0. Let us first take σ_0 to be the central spin. Strictly speaking, the number of such different correlations is $N_k/7$ because of the $2\pi/7$ rotation symmetry. However we find strong evidence that, for k fixed and n large, *all* the $\langle\sigma_0\sigma_k\rangle$ correlations nearly coincide. On the lower, negative x-axis of figure 5, we have chosen $k = 2$ and increased n; the effect of the site alternation with coordination 3 and 4 is clearly visible (see the boundary in figure 1). The correlation inhomogeneities are reduced with increased system size (cf the negative x-axis part of figures 5 and 6).

Boundary behaviour. Now we consider the reference spin σ_0 to be located at the hyperlattice boundary and the spins σ_k at a distance k from σ_0. The dispersion is similar to that already described for the bulk case, though it persists in the large-n limit (see the positive x-axis part in figure 6). The sites with smaller coordination are less correlated, as expected on physical grounds. Therefore the correlations are weakened at the boundary of the hyperlattice.

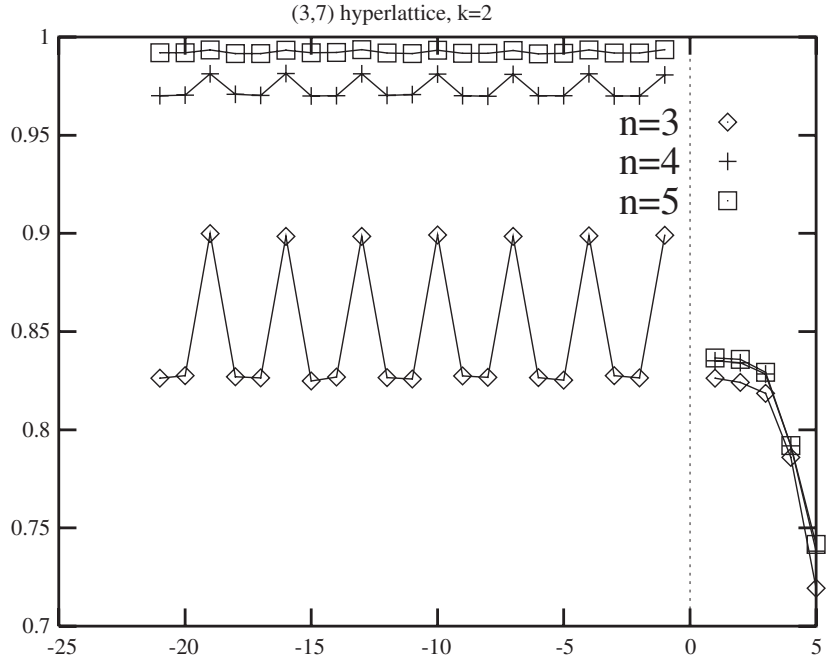

Figure 5. Spin–spin correlations at $T = 1$ for the central (negative x-axis) and a boundary spin (positive x-axis) at a distance $k = 2$ where x is an arbitrary spin index.

6. Magnetization distributions at low temperatures

We now demonstrate slow dynamics at low temperatures in this hyperlattice FIM. Towards this goal, we track the energy and magnetization distributions, comparing results obtained using two sampling methods. The first is a standard heat bath single-spin-flip algorithm that probes configuration space where two configurations are considered neighbours if they differ by exactly one spin. The second one is a cluster algorithm that can go from any configuration to any other in just one step, and is applicable here because of the absence of frustration. We use these two algorithms to probe the structure of the configuration space, analogous to similar studies performed previously on Cayley trees [17, 22]. In both cases, the valleys correspond to magnetic domains in real space (see figure 7). On the hyperlattice, the energy of a magnetic domain scales as the logarithm of its area (see appendix D) while it does not scale with area on the tree.

In figure 8, we present three energy distributions. One was acquired with a cluster algorithm, while the other two were obtained with the single-spin-flip algorithm and 3×10^5 and 4.78×10^5 MCS spins. The three simulations were performed at a temperature $T = 1.4$, below the estimated Bethe–Peierls transition (of the order of the lattice coordination). These three energy distributions are close to the same Gaussian distribution, centred at the mean value of the internal energy, with a width proportional to the specific heat multiplied by the square of the temperature. From this figure it is clear that there are no long timescales present as far as the energy is concerned.

However, the behaviour of the magnetization is rather different. In figure 9 we present three magnetization distributions, determined during the same runs as the internal energy distributions. The three magnetization distributions are *distinctive*. The two distributions

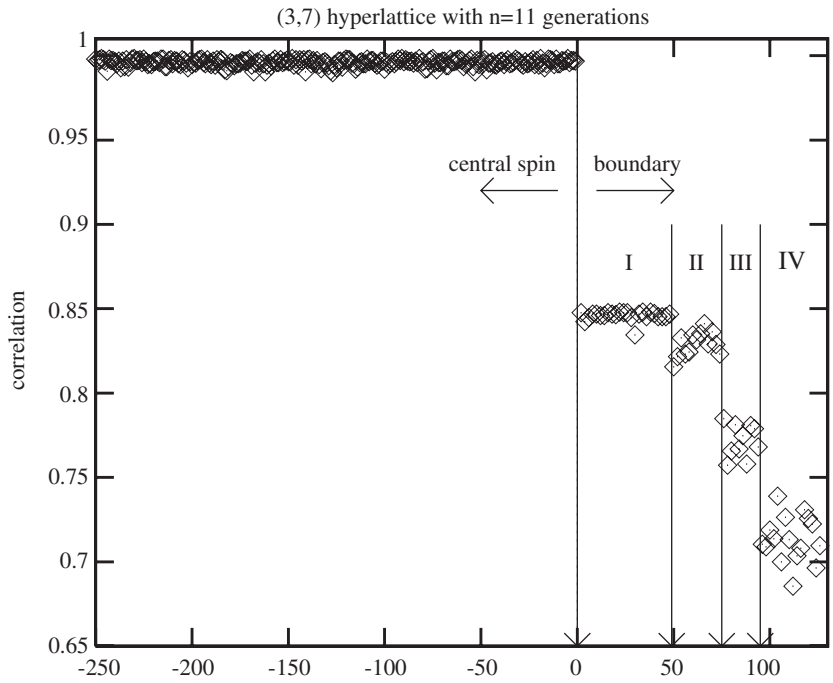

Figure 6. Spin–spin correlations computed for the *central* and a boundary spin at a distance $k = 7$.

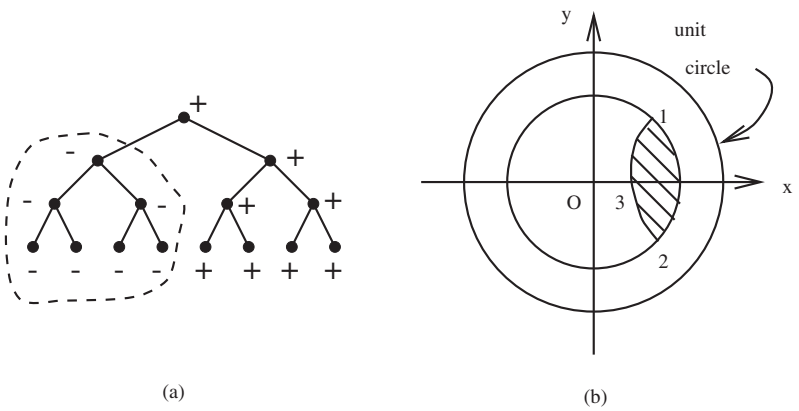

Figure 7. Magnetic domains (*a*) on the tree, and (*b*) on the hyperlattice. The geodesic 1–3–2 is perpendicular to the border of the hyperlattice $R\exp(\mathrm{i}\phi)$. Point 1 is $R\exp(\mathrm{i}\theta)$. Point 2 is $R\exp(-\mathrm{i}\theta)$.

obtained using the single-spin-flip algorithm are *bimodal* whereas the distribution obtained with a cluster algorithm is *unimodal*. For other runs, with fewer statistics, the magnetization distribution with the single-spin-flip algorithm was found to be multimodal, with three or more maxima. This suggests the existence of energy barriers which trap the system with single-spin dynamics. These simulations provide evidence that the low-temperature dynamics are slow. The glass crossover temperature corresponds to the correlation length being comparable to the

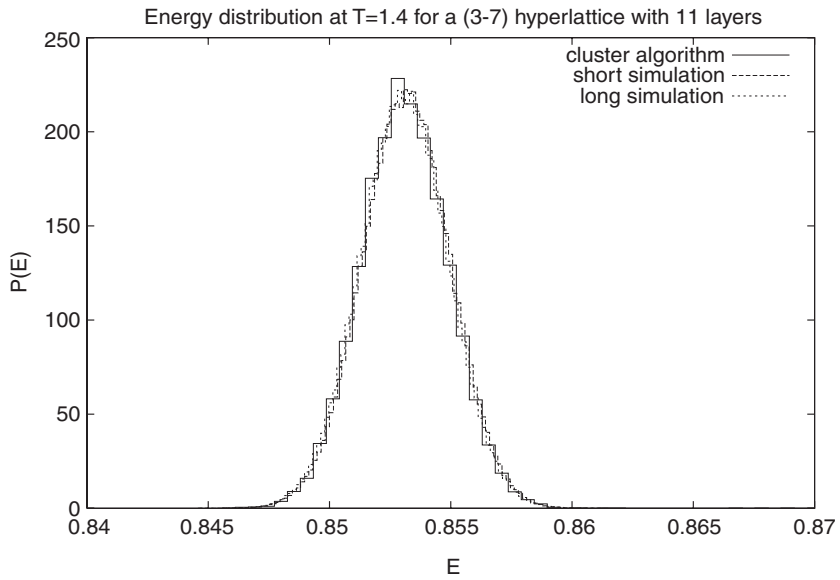

Figure 8. Energy distribution computed at $T = 1.4$ using single-spin-flip cluster algorithms where 'long simulation' and 'short simulation' curves correspond to 47 800 and 300 000 MCS/spins respectively; the 'cluster algorithm' curve was obtained with 10 200 updates of the cluster algorithm.

system size. Also the magnetization distributions are broad at low temperature (see figure 9) for the hyperlattice, similar to that found for the Cayley tree [17]; this is an indication of relaxation on many timescales. This is because of the stability of a Griffiths phase on the entire lattice, at a temperature set by the boundary Bethe–Peierls transition (see appendix E).

7. Discussion

In summary, we have studied the nearest-neighbour FIM on tilings embedded in hyperbolic surfaces with negative curvature, often beginning with the special case of Cayley trees. We have identified two mean-field transitions in these systems, associated with ordering of the bulk and the boundary spins as a function of decreasing temperature. These two transitions can be understood in terms of the local metric properties of the lattice, specifically by the distinct scaling of sites with distance from the boundary and bulk spins. We believe that these two transitions will be characteristic of *any* short-range ferromagnetic model residing on a planar surface with globally negative curvature independent of lattice specifics or the nature of the spin order parameter.

In order to satisfy the criterion of 'global negative curvature', at large length scales the resident lattice should be embedded on a surface with a negative (not necessarily constant) curvature instead of on a Euclidean plane. For instance, we could imagine models with a fluctuating metric. As a simple example, we could consider a recursive random lattice in which the sites have a coordination z with a given probability $P(z)$. The sites with $z = 2$ have the local environment of an Ising chain, and the sites with $z \geqslant 3$ have local branching. The bulk Bethe–Peierls transition is found to be $\langle\langle z-1\rangle\rangle \tanh(\beta_{\text{bulk}} J) = 1$, whereas the boundary transition corresponds to $\sqrt{\langle\langle z-1\rangle\rangle} \tanh(\beta_{\text{bound}} J) = 1$. Both transitions occur at a finite temperature as soon as $\langle\langle z\rangle\rangle > 2$, in which case the metric is globally hyperbolic.

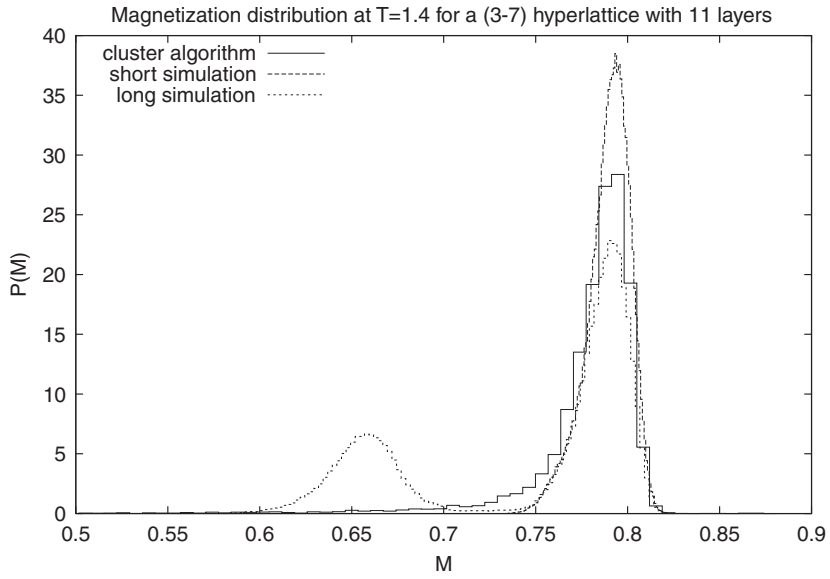

Figure 9. Magnetization distribution computed at $T = 1.4$ using single-spin-flip and cluster algorithms where 'long simulation' and 'short simulation' curves correspond to 47 800 and 300 000 MCS/spins respectively; the 'cluster algorithm' curve was obtained with 10 200 updates of the cluster algorithm. The left peak occurs for the longer simulation.

One can also question how the hyperbolic/Euclidean transition would operate in a continuous model in the limit of a large curvature radius $\mathcal{R} \gg 1$. Such lattices would be obtained as tesselations of negative curvature surfaces, in the limit where the lattice spacing is far below the curvature radius. These lattices could not be constructed using a single type of regular polygon like the ones considered here. The bulk and boundary Bethe–Peierls transitions would be of order $1/\mathcal{R}$ while Euclidean physics would develop below the length scale $\mathcal{R}$. Strictly speaking, the Euclidean phase transition occurs only when $\mathcal{R} = +\infty$. However, when the correlation length is smaller than the curvature radius, the system behaves like a Euclidean system. Therefore, in the presence of a small curvature, pronounced maxima are expected in the susceptibility. The expected behaviour is summarized in figure 10. Again we emphasize that we expect this phase behaviour for ferromagnetic models residing on hyperboloids independent of the details of the spin order parameter. For Cayley trees, it has been shown that the nearest-neighbour xy model displays similar physics (i.e. mean-field transition) to its Ising counterpart [17]. For a general hyperlattice, we expect two mean-field transitions for short-range xy models since there exist loops and two species of spin (boundary and bulk), as in the Ising case. As was done in this paper, these transitions would be obtained by comparing the exponential decay of the correlations to the growth in the number of sites with distance; this would be interesting to verify.

The physics of the low-temperature behaviour of the hyperlattice FIM is determined by the formation of droplet-like excitations nucleating from the boundary. These rare fluctuations do not affect the specific heat (section 3), but do lead to a broad magnetization distribution reflecting a wide spectrum of relaxation timescales. Such Griffiths phases are usually associated with dilute ferromagnets with spatial inhomogeneity. In the models we have studied here there is no intrinsic disorder; however, there are two distinct site species, a feature that contributes to favouring droplet formation. Indeed here we report a diverging susceptibility per site at the

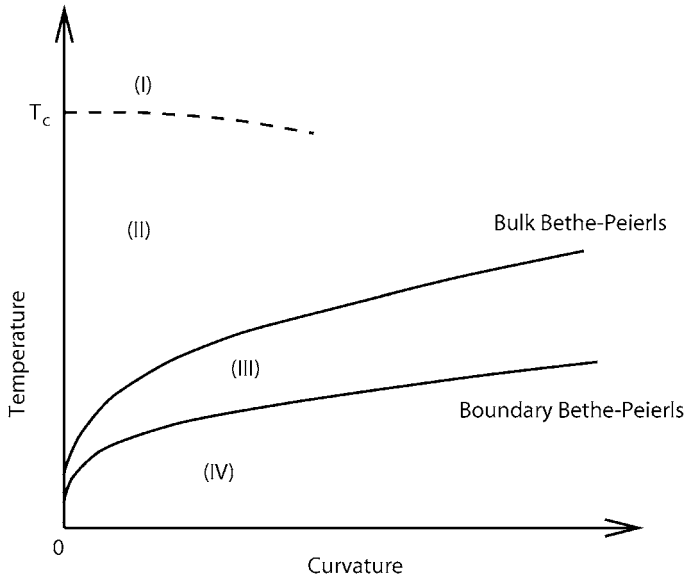

Figure 10. (Curvature, temperature) phase diagram. T_c is the critical temperature of the Euclidean model. The dashed curve is a cross-over between the Euclidean and non-Euclidean model, occurring only with a small curvature radius (the corresponding lattices are not regular hyperlattices like those studied here). Region (I) is the paramagnet. Region (II) corresponds to algebraic correlations below the curvature radius $\mathcal{R}$, and exponential correlations above $\mathcal{R}$. The solid curves are the bulk and boundary Bethe–Peierls transitions, determined as $\xi_T = \mathcal{R}$ and $2\mathcal{R}$ respectively. Note that ξ_T is related to the exponential decay of the correlations above the curvature radius, and *not* to the behaviour of the correlations below the curvature radius. Region (IV) corresponds to the Griffiths phase of the entire lattice.

boundary transition (see appendix E), a characteristic shared with random ferromagnets with correlated disorder[4]. Similarly divergences are reported for quantum disordered magnets, where the randomness is correlated in the time dimension. To our knowledge, this is the first time a Griffiths phase has been identified in a regular magnetic system with loops; furthermore the identification of slow dynamics in a short-range system at low temperatures is very encouraging. For instance the behaviour of the magnetization distribution in figure 9 is reminiscent of the broad overlap distribution in spin glasses [42]. The relaxation time is however finite, a feature reminiscent of glass dynamics. Similarly to slow relaxation in dilute magnets [18], the short-time dynamics may violate the fluctuation dissipation theorem [43] while the long-time dynamics is likely to be an equilibrium dynamics.

Though motivated by experiment, our chosen lattices of study are somewhat removed from the structures commonly observed in nature. However perhaps we can close by attempting to reconnect with experiment. In particular, we have identified Griffiths phases in ferromagnetic models residing on hyperlattices. Though this phenomenon has been discussed extensively in the theoretical literature, it has not yet been conclusively identified in the laboratory[5]. For example, there have been claims in random-field materials [44], but they remain controversial due to plausible alternative interpretations of the data [45]. Perhaps Josephson junction arrays fabricated in a hyperlattice topology would provide a promising setting for the observation of

[4] RM thanks P Pujol for a discussion on this point.

[5] PC thanks J A Mydosh for discussions of experimental attempts at observing Griffiths phases.

this well discussed phenomenon. In this artificial network, a junction is located at each link of the hyperlattice; the short superconducting wires have a phase ϕ_i with a Hamiltonian

$$H = E_J \sum_{\langle i,j \rangle} [1 - \cos(\phi_i - \phi_j)]$$

where the ground-state configurations correspond to a uniform $\phi_i = 0$ and E_J is an energy scale associated with a junction. If this array were placed in a time-dependent transverse magnetic field, the low-frequency part of the resulting ac susceptibility [46] should provide a useful probe for the slow dynamics associated with the Griffiths phase.

In order for our ideas to be applicable to the Josephson hyperlattice, they should not display a vortex binding–unbinding transition. Assuming that the nature of the spin order parameter is not important, we can apply some of our previous expressions to check this. The phase at a distance d from a given bulk vortex scales as $\phi_{\text{bulk}}(l) \sim 4\exp(-2l)$, where we have used the expression equation (7) for the number of sites at a given distance l. The energy of a junction a distance d from a bulk node $\frac{1}{2}E_J[\phi(d)]^2$, leading to the total vortex energy $E_{\text{bulk}} = 2\pi E_J$. It is remarkable that this quantity is *finite*, while it diverges logarithmically with distance on the square lattice. Similarly, the energy of a vortex at the boundary is found to be $E_{\text{bound}} = 2\pi^2 E_J$, again a finite quantity. As a consequence, on the hyperlattice, there is no Kosterlitz–Thouless transition associated with the unbinding of vortex–antivortex pairs. We note that an identical conclusion was reached for two-dimensional Coulomb systems residing on a surface of constant negative curvature [47]; this agreement gives us further confidence in our conjecture about the universal nature of the phase behaviour that we have identified.

Acknowledgments

RM acknowledges a fruitful discussion with A Comtet, S Nechaev and R Voituriez.

Appendix A. Number of sites at a given distance on the tree

We consider a site at generation m on a tree and calculate the number of sites $N_m(l)$ at a given distance l from the site at generation m. This is given by the prefactor of the term x^l in the expansion of the susceptibility in powers of $x = \tanh(\beta J)$:

$$T\chi_{\text{BP}}^{\text{tree}}(m) = \frac{1 - [(z-1)x]^{n-m+1}}{1-(z-1)x} + \sum_{k=0}^{m-1} x^{m-k}[1 + (z-2)x + (z-2)(z-1)x^2 + \cdots + (z-2)(z-1)^{n-k-1}x^{n-k}]. \tag{A.1}$$

Equation (10) has been obtained by summing the series in equation (A.1). First the sum $\sum_{l=0}^{n-m}[(z-1)z]^l$ gives rise to $(z-1)^l$ sites at a distance $0 \leqslant l \leqslant n-m$. Next, the sum $\sum_{k=0}^{m-1} x^{m-k}$ results in one site at a distance $1 \leqslant l \leqslant m$. The remaining terms give rise to $(z-2)(z-1)^{l-m+k-1}$ sites at a distance l, with $0 \leqslant k \leqslant m-1$ and $m-k+1 \leqslant l \leqslant n+m-2k$. We therefore need to distinguish between two cases: case (1) $m \geqslant [(n-1)/2]$ and case (2) $m \leqslant [(n-1)/2]$, with $[\cdots]$ the integer part.

Case 1: $m \geqslant [(n-1)/2]$. We should compare l with $n-m$ and $m+1$. We find three cases:

(i) $l \leqslant n-m$. The number of sites at distance l is $(z-1)^l - 1$.
(ii) $n-m \leqslant l \leqslant m+1$. The number of sites at distance l is $(z-1)^{[(n-m+l)/2]} - 1$.
(iii) $m+1 \leqslant l$. The number of sites at distance l is $(z-1)^{[(n-m+l)/2]} - (z-1)^{l-m-1}$.

Case 2: $m \leqslant [(n-1)/2]$. We compare again l with $n-m$ and $m+1$:

(i) $l \leqslant m+1$. The number of sites at distance l is $(z-1)^l - 1$.
(ii) $m+1 \leqslant l \leqslant n-m$. The number of sites at distance l is $(z-1)^l - (z-1)^{l-m-1}$.
(iii) $n-m \leqslant l$. The number of sites at distance l is $(z-1)^{[(n-m+l)/2]} - (z-1)^{l-m-1}$.

Therefore at large distance the number of sites at a distance l from a given site at generation m scales as $N_m(l) \sim (z-1)^{l/2}$ if $m \geqslant [(n-1)/2]$. This scaling should be compared with the exponential decay of the correlations $\langle \sigma_i \sigma_j \rangle \sim \exp(-d_{i,j}/\xi_T)$ and leads to a boundary transition at a temperature T' given by $(z-1)\tanh^2(\beta' J) = 1$. This transition occurs whenever $n-m$ is finite in the limit $n \to +\infty$.

Appendix B. Percolation on the tree: generalized Bethe–Peierls limit

We would like to illustrate the different behaviour of the generalized Bethe–Peierls transitions on the example of bond percolation where the same phenomenon occurs as in the case of ferromagnetism. We denote by $P_n^{BP}(M)$ the probability of finding M sites (a mass M) in the cluster containing the top site of a tree with n generations. We have

$$P_{n+1}(M) = \sum_{\theta_1} \cdots \sum_{\theta_{z-1}} \sum_{M_1} \cdots \sum_{M_{z-1}} \prod_{i=1}^{z-1} P_n(M_i) \prod_{i=1}^{z-1} p(\theta_i) \delta\left(M - \sum_{i=1}^{z-1} \theta_i M_i - 1 \right)$$

with $\theta_i = 1$ with a probability $p(1) = \mu$ and $\theta_i = 0$ with a probability $p(0) = 1-\mu$. The average number of sites in the cluster containing the top spin of a tree with n generations is iterated as $\tilde{M}_{m+1} = (z-1)\mu \tilde{M}_n + 1$. The fixed point value is $\tilde{M}^* = 1/(1-(z-1)\mu)$ and diverges at the bulk percolation threshold $\mu_P^0 = 1/(z-1)$.

We now consider the number of sites $M(\mathcal{T}_m)$ in a cluster containing the point $\mathcal{T}_m$ in the presence of n generations (see figure 3). We find

$$M(\mathcal{T}_m) = \frac{[(z-1)\mu]^{n-m+1} - 1}{(z-1)\mu - 1} + \frac{(z-2)\mu^2}{(z-1)\mu - 1} \left([(z-1)\mu]^{n-m+1} \frac{[(z-1)\mu^2]^m - 1}{(z-1)\mu^2 - 1} - \frac{1-\mu^m}{1-\mu} \right) \tag{B.1}$$

of the same form as equation (10). If $n, m \to +\infty$ with $n-m$ constant, the cluster size containing the vertex $\mathcal{T}_m$ does not diverge at the bulk percolation threshold μ_P^0 while it diverges at a larger percolation threshold $\mu_P' = 1/\sqrt{z-1}$. If $n \to +\infty$ and $n-m$ grows faster than n, we find a percolation transition at the bulk percolation threshold μ_P^0. Therefore, similarly to ferromagnetism, percolation shows a different behaviour depending on how the Bethe–Peierls limit is taken. The boundary percolation threshold μ_P' is larger than the bulk percolation threshold μ_P^0.

Appendix C. Number of sites at a given distance from a boundary site on the hyperlattice

We consider a finite-size disc $|z| < R$ with the hyperbolic metrics equation (1), and calculate the length of the set of points at a distance d from the boundary site at coordinate R. This set of points is represented by the circle $x_0 + R_0 \exp(i\phi)$ (see equation (4)), which intersects the boundary $|z| = R$ at the points $z^{\pm} = x_0 + iR_0 \exp(\pm i\phi_0)$, with

$$\cos\phi_0 = \frac{\tanh d}{2R(1-\tanh^2 d)} (1 + (-3 + \tanh^2 d) R^2 + (\tanh^2 d) R^4).$$

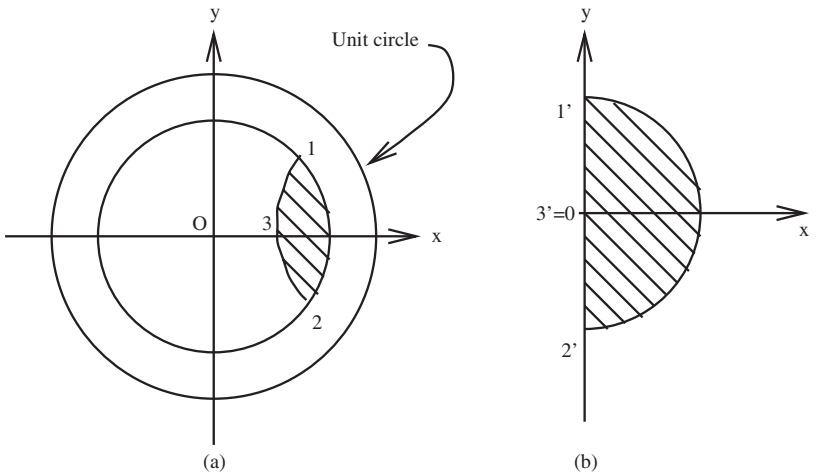

Figure D.1. Isometry transform of the droplet excitation of the hyperlattice. (*a*) The original droplet, and (*b*) the transformed droplet. The isometry is chosen such that the segment $1'$–$3'$–$2'$ is on the y axis with $3'$ at the origin. Point 1 is $R\exp(\mathrm{i}\theta)$; point 2 is $R\exp(-\mathrm{i}\theta)$. Point $1'$ is $\mathrm{i}\rho$; point $2'$ is $-\mathrm{i}\rho$.

A straightforward calculation leads to the length of the arc z^+–z^-:

$$\mathcal{L}_{\text{bound}} = \int \sqrt{g(z)}R_0\,\mathrm{d}\phi = \frac{4\tanh d}{1-\tanh^2 d}\tan^{-1}\left[\sqrt{\frac{2R-(1+R^2)\tanh d}{2R+(1+R^2)\tanh d}}\right].$$

In the relevant regime $1 \ll d \ll \tanh^{-1} R$ with $R \simeq 1$, we find $\mathcal{L}_{\text{bound}} \sim \exp(d)$. This boundary behaviour should be contrasted with the bulk behaviour $\mathcal{L}_{\text{bulk}} \sim (\pi/2)\exp(2d)$ (see equation (7)).

Appendix D. The length of magnetic domains

We show that the length of the droplet excitations shown in figure 7(*b*) is proportional to the logarithm of its area. The difference from the calculation in appendix C is that we consider here the geodesics 1–3–2 corresponding to the physical situation where the energy of the domain wall is minimized.

To calculate the shaded area in figures 7(*b*) and D.1(*a*), we use the transformation $z \to z' = (az+b)/(bz+a)$ with a and b real numbers, to map the domain in figures D.1(*a*) and 7(*b*) into the domain on figure D.1(*b*). Imposing point 1 to be transformed into $1'$ at coordinate $\mathrm{i}\rho$ leads to

$$\alpha \equiv \frac{b}{a} = -\frac{R\cos\theta(1+\rho^2)}{1+\rho^2R^2+2\rho R\sin\theta}$$

with

$$\rho = \frac{1}{2R\sin\theta}(-(1-R^2)+((1-R^2)^2+4R^2\sin^2\theta)^{1/2}).$$

The area element is found to be

$$\mathrm{d}\mathcal{A} = g(r')\,\mathrm{d}r'\,\mathrm{d}\theta' = \frac{r}{2(1-r^2)}\,\frac{(1+\alpha^2)r + (r^2+1)\alpha\cos\theta}{1+\alpha^2r^2+2\alpha r\cos\theta}\,\mathrm{d}\theta.$$

A straightforward integration over θ leads to

$$\mathcal{A} = \frac{\theta}{2}\left(\frac{1+R^2}{1-R^2}\right) + \frac{\alpha^2R^2-1}{|1-\alpha R|}\tan^{-1}\left(\left|\frac{1-\alpha R}{1+\alpha R}\right|\tan\left(\frac{\theta}{2}\right)\right).$$

When $R \simeq 1$, we have $\mathcal{A} \sim \theta/[2(1-R)]$. The length of the line 1–3–2 is $\mathcal{L} = \frac{1}{2}\ln[(1+\rho)/(1-\rho)] \sim -\frac{1}{2}\ln(1-R)$. The scaling between the area and length of a magnetic domain in the limit $R \to 1$ is finally found to be $\mathcal{A} \sim \frac{\theta}{2}\exp(2\mathcal{L})$: the area is exponentially large in the boundary length.

Appendix E. Total susceptibility: Griffiths transition

We derive the total susceptibility of the tree and hyperlattice models. The susceptibility of both models diverges below the Griffiths temperature set by the local transition temperature of the boundary.

E.1. Tree model

The susceptibility of the entire lattice χ_{TOT} is obtained as the sum of the local susceptibilities: $\chi_{\mathrm{TOT}} = \sum_{m=0}^{n}(z-1)^m\chi_m(T)$. First if $T > T'$, the susceptibility per spin behaves like $\chi_{\mathrm{TOT}}/N_n \sim (1+x)^2/[1-(z-1)x^2]$, and diverges at the temperature T'. Now if $T < T'$, the susceptibility per spin behaves like $\chi_{\mathrm{TOT}}/N_n \sim [(z-1)x^2]^n$, an infinite quantity in the limit $n \to +\infty$.

E.2. Hyperlattice model

We first estimate the local susceptibility of the hyperlattice with a finite size $|z| < R$ at the point represented by a real number x, and we assume the correlations to be uniform as discussed in section 5 of the main body of the text. We note $d = d(x, R) = \tanh^{-1}[(R-x)/(1-xR)]$ the distance between the points x and R, and $D = \tanh^{-1}[(R+x)/(1+xR)]$ the distance between the points x and $-R$. Based on figure 4 and appendix C, we approximate the growth of the number of sites $\mathcal{N}(l)$ at a distance l from the point x as follows: (i) $l < d$ (bulk behaviour), $\mathcal{N}(l) \simeq (\pi/2)\exp(2l)$; (ii) $d < l < D$ (boundary behaviour), $\mathcal{N}(l) \simeq (\pi/2)\exp(l+d)$. The local susceptibility is found to be

$$\begin{aligned} T\chi(x) &\simeq \int_0^D \mathcal{N}(l)\exp(-l/\xi_{\mathrm{T}})\,\mathrm{d}l \\ &= \frac{\pi}{2}\frac{1}{2-1/\xi_{\mathrm{T}}}[\mathrm{e}^{(2-\frac{1}{\xi_{\mathrm{T}}})d}-1] + \frac{\pi}{2}\frac{1}{1-1/\xi_{\mathrm{T}}}\mathrm{e}^{d}[\mathrm{e}^{(1-\frac{1}{\xi_{\mathrm{T}}})D} - \mathrm{e}^{(1-\frac{1}{\xi_{\mathrm{T}}})d}]. \end{aligned} \tag{E.1}$$

In the case of the central spin $x = 0$, we find a susceptibility diverging at $\xi_{\mathrm{T}} = 1/2$. In the case of a boundary site $x = R$, we find a susceptibility diverging at $\xi_{\mathrm{T}} = 1$, consistent with the behaviours obtained in the main text of this paper. The total susceptibility is obtained as the sum of the local susceptibilities, equation (E.1):

$$\chi_{\mathrm{TOT}} = \int_0^R 2\pi x g(x)\chi(x)\,\mathrm{d}x. \tag{E.2}$$

We note $R = 1-\epsilon_R$, and expand the susceptibility equation (E.2) in the parameter $\epsilon_R \ll 1$. The number of sites N_{s} scales as ϵ_R^{-1}. If $\xi_{\mathrm{T}} < 1$, the susceptibility per site is found not to scale

with N_s. If $\xi_T > 1$, the susceptibility per site is found to scale as $\epsilon_R^{-1+1/\xi}$, an infinite quantity in the limit $\epsilon_R \to 0$.

Therefore, the tree and hyperlattice models show the same behaviour: the susceptibility per site is infinite below the Griffiths transition temperature T'. The Griffiths temperature T' is equal to the temperature of the boundary Bethe–Peierls transition. Physically, this originates because of the finite fraction of spins at the boundary: the boundary dominates the behaviour of the total susceptibility.

References

[1] Anderson P W 1979 *Ill-Condensed Matter* ed R Balian, R Maynard and G Toulouse (Amsterdam: North-Holland) pp 162–258
[2] Ramakrishnan T and Raj Lakshmi M (ed) 1987 *Non-Debye Relaxation in Condensed Matter* (Singapore: World Scientific)
[3] Mydosh J A 1993 *Spin Glasses: an Experimental Introduction* (London: Taylor and Francis)
[4] Aeppli G and Chandra P 1997 *Science* **275** 177
[5] Ramirez A P 2000 *Handbook of Magnetic Materials* (Amsterdam: North-Holland)
[6] Willis A S, Dupuis V, Vincent E, Hammann J and Calemczuk R 2000 *Preprint* cond-mat/0001344
[7] Chandra P, Coleman P and Ritchey I 1993 *J. Physique* I **3** 591
[8] Bouchaud J P, Cugliandolo L F, Kurchan J and Mézard M 1998 Out-of-equilibrium dynamics in spin-glasses and other glassy systems *Spin Glasses and Random Fields* ed A P Young (Singapore: World Scientific)
[9] Bray A J and Moore M A 1986 *Heidelberg Colloquium on Glassy Dynamics and Optimization* ed L Van Hemmen and I Morgenstern (Berlin: Springer)
Bray A J and Moore M A 1987 *Phys. Rev. Lett.* **58** 57
[10] Fisher D S and Huse D A 1986 *Phys. Rev. Lett.* **56** 1601
Fisher D S and Huse D A 1988 *Phys. Rev.* B **38** 373
[11] Griffiths R B 1969 *Phys. Rev. Lett.* **23** 17
[12] Nieuwenhuizen Th M 1989 *Phys. Rev. Lett.* **63** 1760
[13] Weissman M 1993 *Rev. Mod. Phys.* **65** 829
[14] Bray A J 1994 *Adv. Phys.* **43** 357
[15] Alberici-Kious F, Bouchaud J P, Cugliandolo L F, Doussineau P and Levelut A 1998 *Phys. Rev. Lett.* **81** 4987
[16] Kirkpatrick S 1979 *Les Houches Summer School on Ill Condensed Matter* ed R Balian, R Maynard and G Toulouse (Amsterdam: North-Holland)
[17] Mélin R 1996 *J. Physique* I **6** 1435
[18] Butaud P and Mélin R 1998 *J. Phys. A: Math. Gen.* **31** 5203
[19] Balazs N L and Voros A 1986 *Phys. Rep.* **143** 109
[20] Gutzwiller M C 1990 *Chaos in Classical and Quantum Dynamics* (New York: Springer)
[21] Comtet A, Nechaev S and Voituriez R 2000 *Preprint* cond-mat/0004491
[22] Mélin R, Anglès d'Auriac J C, Chandra P and Douçot B 1996 *J. Phys. A: Math. Gen.* **29** 5773
[23] Anglès d'Auriac J C, Preissman M and Sebő A 1997 *J. Math. Comput. Modelling* **26** 1
[24] McCoy B M and Wu T T 1968 *Phys. Rev.* **176** 631
[25] Clark T E, Menikoff R and Sharp D H 1980 *Phys. Rev.* D **22** 3012
[26] Mosseri R and Sadoc J F 1982 *J. Physique Lett.* **43** L249
[27] Rietman R, Nienhuis B and Oitmaa J 1992 *J. Phys. A: Math. Gen.* **25** 6577
Rietman R 1993 Yang Baxter equations, hyperlattices and loop models *PhD Thesis* Amsterdam University
[28] Swendsen R H and Wang J S 1986 *Phys. Rev. Lett.* **57** 2606
Swendsen R H and Wang J S 1987 *Phys. Rev. Lett.* **58** 86
See also Swendsen R H, Wang J S and Ferrenberg A M 1992 *The Monte Carlo Method in Condensed Matter Physics (Topics in Applied Physics vol 71)* ed K Binder (Berlin: Springer)
[29] Bethe H A 1935 *Proc. R. Soc.* A **150** 552
[30] Peierls R 1936 *Proc. Camb. Phil. Soc.* **32** 477
[31] Domb C 1960 *Adv. Phys.* **9** 145
[32] Baxter R J 1982 *Exactly Solved Models in Statistical Mechanics* (New York: Academic)
[33] Thorpe M F 1982 *Excitations in Disordered Solids (NATO Advanced Study Institute Series B)* ed M F Thorpe (New York: Plenum) p 85
[34] Thompson C J 1982 *J. Stat. Phys.* **27** 441

[35] Itsykson C and Drouffe J M 1989 *Statistical Field Theory* vols 1 and 2 (Cambridge: Cambridge University Press)
[36] Monthus C and Texier C 1996 *J. Phys. A: Math. Gen.* **29** 2399
[37] Cassi D 1989 *Europhys. Lett.* **9** 627
[38] Giacometti A 1995 *J. Phys. A: Math. Gen.* **28** L13
[39] Helfand E and Pearson D S 1983 *J. Chem. Phys.* **79** 2054
[40] Muller-Hartmann E and Zittartz J 1974 *Phys. Rev. Lett.* **33** 893
Muller-Hartmann E and Zittartz J 1975 *Z. Phys.* B **22** 59
[41] Turban L 1980 *Phys. Lett.* A **78** 404
[42] Marinari E, Parisi G, Ricci-Tersenghi F and Ruiz-Lorenzo J J 1998 *J. Phys. A: Math. Gen.* **31** 2611
[43] Crisanti A, Horner H and Sommers H J 1993 *Z. Phys.* B **92** 257
Cugliandolo L F and Kurchan J 1993 *Phys. Rev. Lett.* **71** 173
Nieuwenhuizen Th M 1998 *Phys. Rev. Lett.* **80** 5580
[44] Binek C and Kleemann W 1994 *Phys. Rev. Lett.* **72** 1287
Binek C, Kuttler S and Kleeman W 1995 *Phys. Rev. Lett.* **75** 2412
[45] Dotsenko V I 1994 *J. Phys. A: Math. Gen.* **27** 3397
[46] Chandra P, Feigelman M V, Ioffe L B and Kagan D M 1997 *Phys. Rev.* B **56** 11 553
[47] Jancovici B and Tellez G 1998 *Preprint* cond-matt/9801322